

Charge transfer, polarization, and relaxation effects on the Auger line shapes of Si

D. E. Ramaker

*Chemistry Division, Naval Research Laboratory, Washington, D.C. 20375
and Chemistry Department, George Washington University, Washington, D.C. 20052*

F. L. Hutson

Chemistry Department, George Washington University, Washington, D.C. 20052

N. H. Turner

Chemistry Division, Naval Research Laboratory, Washington, D.C. 20375

W. N. Mei

Chemistry Department, George Washington University, Washington, D.C. 20052

(Received 7 March 1985; revised manuscript received 21 October 1985)

The Auger line shapes of Si are quantitatively interpreted noting particularly the core-hole screening effects as exhibited through charge transfer, polarization, and atomic relaxation. The KL_1V , $KL_{2,3}V$, and $L_1L_{2,3}V$ line shapes reflect a core-hole-screened density of states (DOS) consistent with the core hole in the final state of these processes. A DOS appropriate for the screened core hole is obtained by distorting the theoretical DOS for the ground state utilizing the Green's function for a tight-binding Hamiltonian and a central-cell potential. Comparison of the $L_{2,3}VV$ and KVV line shapes reveal large differences. These differences are discussed in the context of surface effects, intrinsic and extrinsic plasmon losses, and final-state shakeoff. The $L_{2,3}VV$ and KVV line shapes also suggest some distortion effects due to final-state hole correlation. The $KL_{2,3}L_{2,3}$ line shape is interpreted in the context of similar line shapes for Na, Mg, Al, and P; all show plasmon losses and, except for P, initial-state shakeoff contributions.

I. INTRODUCTION

The Auger process is a complicated dynamical process exhibiting several interesting phenomena.¹ One of these is atomic relaxation and electron screening in response to either the initial- or final-state core holes. In an effort to develop a semiempirical approach to near quantitative Auger line-shape interpretation, we have previously developed a final-state rule (FS rule) which provides a simple prescription for including some of the effects of core-hole screening in the Auger line shape.² In this work, we utilize the FS rule to consistently interpret the CCV , CVV , and CCC (C represents core, V represents valence) Auger line shapes of Si.

The well-characterized Auger line shapes of Si provide an ideal system for testing the FS rule and sorting out screening effects in the Auger process. The KL_1V , $KL_{2,3}V$, $L_1L_{2,3}V$, and $L_{2,3}VV$ line shapes have been extensively studied and reported in the literature.³⁻⁹ The KL_1V , $KL_{2,3}V$, and $L_1L_{2,3}V$ line shapes have been shown to exhibit large core-hole screening effects, consistent with a final-state core hole in these CCV line shapes,⁹ but quantitative interpretations of these line shapes have not been reported in the context of core-hole screening.³⁻⁸ Much controversy has existed in the literature concerning the interpretation of the $L_{2,3}VV$ line shape and the apparent lack of ss and sp contributions (s and p refer to the local angular momentum of the final-state valence holes created by the Auger process) to the line shape.⁴⁻⁸ This

lack of ss and sp intensity has been attributed to atomic Auger matrix element effects^{4,5,7,8} or to the nature (local versus bonding) of the electronic charge sampled by the Auger process.⁶ In this work we shall attempt to show that the apparent lack of ss and sp contributions in the CVV line shapes ($L_{2,3}VV$ and KVV) arises either from the core-hole screening response in the initial state or from surface effects. The KVV line shape to our knowledge has not been previously reported; we present qualitative results for the KVV line shape in this work (Sec. II). The $KL_{2,3}L_{2,3}$ (CCC) line shape is obtained also in this work and discussed in the context of core-hole screening effects.

The response of the valence electrons to the creation of a core hole can take several forms. In simple atoms, the orbitals usually contract around a core hole, this is normally referred to as atomic relaxation. In molecules and solids, the bonds also polarize, i.e., electron density in a bonding orbital flows toward the core hole, in an antibonding orbital it flows away from the hole. In the event that the bonding and antibonding orbitals (bands in the case of a solid) are not completely filled, a net charge transfer to the atom with the core hole results. In some systems the screening charge may be sufficiently polarized as to produce a localized or excitonic state below the valence or conduction band.¹⁰⁻¹² The screening may also involve a more nonlocal accumulation of charge around the core hole (plasmon) or create electron-hole pairs giving rise to an edge singularity.¹³

In this work, all of these screening effects are either ex-

hibited in the Si Auger line shapes and/or included in our theoretical interpretation. The Si Auger line shapes will be interpreted utilizing the Si theoretical density of states (DOS) as reported by Papaconstantopoulos and Economou using a Slater-Koster Hamiltonian (Sec. III).¹⁴ A Green's-function approach derived for the tight-binding Hamiltonian is used to distort the ground-state DOS giving the proper polarization and charge transfer of the valence electrons in response to the core hole.¹⁵ Introducing the OFS rule ("orthogonalized" final-state rule) will be discussed in Sec. III but not utilized in this work) accounts for electron-hole pair excitations and the edge singularity.² Plasmon effects are not explicitly accounted for in the theory but are clearly evident in the $KL_{2,3}L_{2,3}$ line shape and perhaps the KVV line shape. Atomic relaxation introduces initial- and final-state shake off. These shakeoff effects must be interpreted as a breakdown in the validity of the FS rule as we applied it in this work; however, they may be included in the OFS rule.² It is believed that final-state shakeoff may be exhibited in the CVV line shapes.

II. EXPERIMENT

The KVV Auger spectrum is normally of extremely low intensity. This arises because a Si K core hole may decay via any of the following Auger processes: $KL_{2,3}L_{2,3}$, $KL_{2,3}V$, KL_1V , and KVV , as well as via x-ray emission. Calculations of Chen *et al.* indicate the following relative decay rates, respectively: 1, 0.02, 0.07, 0.002, and 0.165.^{16,17} Thus, roughly only one KVV electron can be expected per 630 K core-hole excitations. This small intensity for the KVV line shape probably accounts for its absence in the literature.

In this work, the KVV line shape was obtained utilizing the Physical Electronics model No. 545 spectrometer. Si samples were cut from a wafer of microelectronics grade. During the data collection, the surface was continuously Ar sputtered at a pressure of 5×10^{-7} Torr to prevent a buildup of SiO_x . The Auger process was initiated via electron excitation at 5 keV and at a current of $\sim 10 \mu A$ in the normal derivative mode with a modulation potential of 4 V. The data were collected from 1765 to 1900 eV over a period of ~ 50 h. Despite the high noise level, the peak at ~ 1846 eV was reproduced in several experiments. A linear background was subtracted from the measured $d[EN(E)]/dE$ line shape. This is shown along with point-by-point integrated results in Fig. 1; integration smooths the data dramatically. A loss spectrum was taken at $E_p \sim 1860$ eV and deconvoluted from this integrated spectrum.^{3,5-7,18} The large width of the elastic peak reflects the poor resolution of the single pass cylindrical mirror analyzer (CMA) ($\Delta E/E \sim 0.005$) at these high energies, and makes the normal deconvolution procedure much more difficult. We found that separating the loss spectrum into two parts, the elastic peak and the loss spectrum, and then deconvoluting the loss part first made it possible to remove the loss contributions from the Auger spectrum easily. Deconvolution of the elastic peak was more difficult, and the iterative van Cittert scheme ultimately introduced extraneous peaks.¹⁹ This was

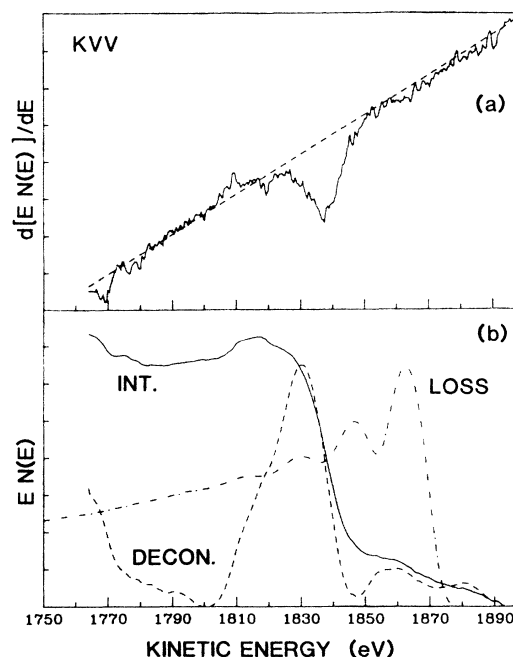


FIG. 1. (a) Derivative ($d[EN(E)]/dE$) KVV Auger spectrum as obtained in this work. The estimated background is shown by the straight line. (b) Integrated spectrum (solid line), the loss spectrum (dot-dashed line) and final deconvoluted KVV line shape (dashed line).

avoided by terminating the iterative scheme earlier, but we believe most of the resolution broadening was removed.

The Si KLL line shape was x-ray excited utilizing continuous bremsstrahlung radiation coming from an Al anode under 8 keV electron bombardment. The use of continuous bremsstrahlung radiation²⁰ for Auger excitation has been previously termed continuous x-ray excited Auger electron spectroscopy (CXAES),^{21,22} but in reality the Auger process is such that no difference should exist between the CXAES and a normal AES line shape using a high energy x-ray line source. In Sec. IV (Fig. 11) we compare the Si KLL line shape obtained in this work with that of Cazaux and Minh Duc,²² who used bremsstrahlung radiation from a W anode. We have smoothed the published data once and both line shapes were deconvoluted with a hypothetical flat and constant "loss" function and zero width elastic peak to remove the background due to the noncharacteristic extrinsic losses.¹⁹ The width of the main line reflects the lifetime of the Si K level, experimental resolution (approximately ~ 1 eV for the McPherson hemispherical analyzer used to take the KLL spectrum in this work), and broadening due to the smoothing procedure.

III. THEORY

A. Final-state rule

The final-state rule for Auger line shapes² is an extension of the FS rule in existence for x-ray emission and absorption.²³⁻²⁵ The FS rule has been previously applied to the CVV Auger line shapes of Na metal.²³ The FS rule

for the Auger process can be stated as follows: In the absence of significant configuration mixing (localization) and shake processes, the initial state determines separately the relative l or l' ($l=s$ or p) Auger intensities; the shape of each contribution is determined by the final density of states.² An OFS rule also has been derived. It has been shown to improve on the FS rule primarily near the threshold where it accounts for some of the edge singularity effects.^{2,26} The Auger intensity $W(\epsilon)$ within the FS and OFS rules can be written in terms of the normal Auger matrix elements,²

$$W_{\text{FS}}(\epsilon) \propto |\langle \varphi_c \bar{\epsilon}_i | r_{12}^{-1} | \varphi_i \bar{\varphi}_j \rangle|^2 R_i R_j, \quad (1)$$

$$W_{\text{OFS}}(\epsilon) \propto |\langle \varphi_c \bar{\epsilon}_i | r_{12}^{-1} | \tilde{\varphi}_i \tilde{\varphi}_j \rangle|^2 R_i R_j. \quad (2)$$

The final-state holes φ_i and $\bar{\varphi}_j$ arise as a result of the Auger process; the Auger electron escapes with energy ϵ_i in the continuum orbital $\bar{\epsilon}_i$, the other electron drops into the core orbital φ_c . $\bar{\varphi}$ indicates orbitals with spin-down, φ indicates those with spin-up. The coefficients R_i , constant in ϵ , are present so that W reflects the initial-state charge population; these R coefficients are defined more fully in Eq. (7) below.

In Eqs. (1) and (2), φ_i and $\tilde{\varphi}_j$ are related by the expression

$$\tilde{\varphi}_i = \varphi_i - \sum_{n(\text{unocc})} S_{in} \varphi'_n - \sum_m S_{im} f'_{im} = \sum_{n(\text{occ})} S_{in} \varphi'_n, \quad (3)$$

where φ'_n are the unoccupied (unocc) band orbitals (from the same band as φ_i) in the presence of the initial-state core hole, and the f'_{im} are all the other unoccupied orbitals (Rydberg, continuum etc.) in the potential of the initial core hole.² In Eq. (3), the $\tilde{\varphi}_i$ orbitals are orthogonalized to all of the unoccupied initial-state orbitals; hence the name orthogonalized FS rule. Projecting out the φ'_n contributions accounts for the particle-hole pair excitations reflected in the edge singularity effects, and the f'_{im} essentially account for atomic relaxation that introduces final-state shakeoff. In practice it is easier to project the φ_i onto the occupied (occ) initial-state orbitals as indicated in Eq. (3), but even this procedure requires a reduction of the infinite band orbital problem to a finite number of cluster orbitals.²⁶ In this work, we utilize only the FS rule which does not require the projection procedure, and hence ignore these two screening effects. No edge singularity effects are evident in the Auger line shapes of Si. We will discuss only qualitatively the final-state shakeoff effects evident in the Si CVV line shapes.

The experimental line shapes, $A(E)$, are quantitatively examined using the equations,

$$A_{CCV}(E) = C_S N'_S(E) + C_p N'_p(E), \quad (4)$$

$$A_{CVV}(E) = C_{ss} R_s^2 N_s(E) * N_s(E) + C_{sp} R_s R_p N_s(E) * N_p(E) + C_{pp} R_p^2 N_p(E) * N_p(E), \quad (5)$$

where $N_l(E) * N_{l'}(E)$ indicates the fold of the DOS,

$$N_l(E) * N_{l'}(E) = \int N_l(E - \epsilon) N_{l'}(\epsilon) d\epsilon, \quad (6)$$

consistent with the FS rule, $N_l(E)$ is the DOS of the final state without a core hole, $N'_l(E)$ is the screened DOS lo-

cal to a core hole. The R_l factors in Eq. (5) can be defined,

$$R_l = \int_{\text{occ}} N'_l(\epsilon) d\epsilon / \int_{\text{occ}} N_l(\epsilon) d\epsilon. \quad (7)$$

They are the ratio of local charge in the screened initial state to that in the unscreened final state of the CVV Auger process. They appear in Eq. (5) because the FS rule states that the relative intensities of the l' contributions are determined by the initial state. They do not appear in Eq. (4) because both the initial and final states contain a core hole (i.e., the R factors are assumed to be 1). An expression similar to Eq. (4) has been used previously to interpret the CCV Auger line shapes in Na.²³

Equation (5) assumes that final-state hole-hole correlation effects are negligible in the CVV line shapes. In the event that correlation effects are not negligible, the $N_l(E) * N_{l'}(E)$ line shape becomes distorted; this can be included by using the Cini-Sawatzky expression (see Ref. 1 and other references cited therein),

$$N_l''(E) * N_{l'}''(E) = \frac{N_l(E) * N_{l'}(E)}{[1 - UI(E)]^2 + U^2 \pi^2 [N_l(E) * N_{l'}(E)]^2}, \quad (8)$$

where $I(E)$ is the Hilbert transform,

$$I(E) = \int [N_l(E') * N_{l'}(E - E') / (E - E')] dE'. \quad (9)$$

Above, U is the fully screened hole-hole Coulomb repulsion and $N_l'' * N_{l'}''$ and $N_l * N_{l'}$ are the correlated and uncorrelated folds of the DOS, respectively. We shall see in Sec. IV B that small distortion effects are indeed suggested in the Si CVV line shapes.

B. Atomic Auger intensities

The coefficients C_l and $C_{l'}$ are obtained from an optimal fit of the right-hand side of Eqs. (4) and (5) to the experimental line shape. The ratio of the coefficients reflects the ratio of the atomic Auger intensity ratios,

$$\frac{1}{3} C_s / C_p = A_{ccs} / A_{cpp}, \quad (10)$$

$$\frac{1}{9} C_{ss} / C_{pp} = A_{css} / A_{cpp}, \quad (11)$$

$$\frac{1}{3} C_{sp} / C_{pp} = A_{csp} / A_{cpp},$$

where the numerical factors arise to account for the presence of $3p$ orbitals (p_x, p_y, p_z) versus just a single s orbital. The atomic Auger intensities $A_{cl'}$ and A_{cel} , normalized per filled shell, can be obtained empirically and compared with what the line-shape fit indicates. Such a comparison provides a measure of the overall consistency of our line-shape interpretation technique and, hence, also on the validity of the FS rule used in the interpretation.

Figure 2 contains plots of the intensity ratios, A_{ccs} / A_{cpp} , for the KL_1V , $KL_{2,3}V$, and $L_1L_{2,3}$ line shapes. We consider just the KL_1V and $KL_{2,3}V$ plots first. Both theoretical and experimental results are shown. The experimental intensities (except for Ar) have been tabulated by Bakenkov *et al.*²⁷ from the literature. The experimental argon results are from Asplund *et al.*²⁸ and Mackey *et al.*,²⁹ the latter data arising from proton impact rather

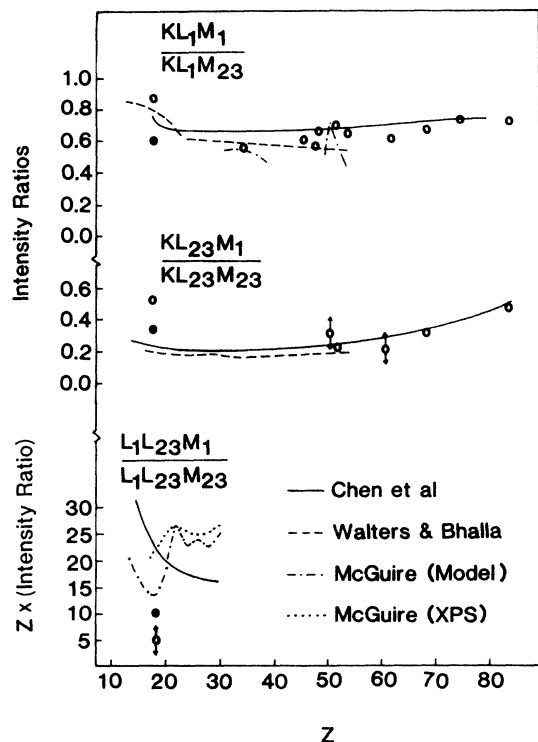


FIG. 2. Plot of the s/p Auger atomic intensity ratios per filled s and p shells for the KL_1V , $KL_{2,3}V$, and $L_1L_{2,3}V$ processes. The s/p ratio for the $L_1L_{2,3}V$ process has been scaled by Z for $Z < 24$, by $Z \times 1.5$ for $Z > 24$ as discussed in the text. The open circles indicate experimental data as tabulated by Babenkov *et al.* (Ref. 27). The solid lines indicate the theoretical results from Chen *et al.* (Ref. 16), the dashed line indicates theoretical results from Walters and Bhalla (Ref. 30), the dotted and dot-dashed lines indicate theoretical results from McGuire (Ref. 31). The data points for Ar are discussed in the text (Refs. 28 and 29).

than electron impact as in all of the other data. Several theoretical calculations of varying degrees of sophistication have also been reported; only the two most recent are shown in Fig. 2. Those of Chen *et al.*¹⁶ have been calculated *ab initio* relativistically from perturbation theory, for frozen orbitals, in the Dirac-Hartree-Slater approach. Walters and Bhalla³⁰ utilized a numerical Hartree-Fock-Slater approach with the Kohn-Sham-Gaspar exchange approximation.

The $L_1L_{2,3}V$ Coster-Kronig (CK) case presents a special problem, both theoretically and experimentally, because of the low CK electron kinetic energy. The low kinetic energy causes the theoretical calculations to show a strong dependence on the estimate of this energy. This has been illustrated for Ar by McGuire³¹ using his approximate Herman-Skillman calculations, where both theoretical model energies and experimental x-ray photoelectron spectroscopy (XPS) binding energies were used in the expression,

$$E_{L_1L_{2,3}M} = E_{L_1} - E_{L_{2,3}} - E_M, \quad (12)$$

to estimate $E_{L_1L_{2,3}M}$. Large differences were seen in the

absolute magnitudes of the CK matrix elements for these two estimates of $E_{L_1L_{2,3}M}$. Figure 2 shows that this causes large differences also in the s/p ratio. More recent theoretical results of Chen *et al.*¹⁶ are based on relativistic relaxed orbital calculations of $E_{L_1L_{2,3}M}$.³² These calculations are expected to give more realistic CK continuum energies and hence also more realistic s/p ratios. In any event, results for only four different values of Z have been reported for each calculation, and the s/p ratio varies widely over this range. Analysis of the results of Chen *et al.*¹⁶ reveals this large variation arises for two reasons. The $L_1L_2M_1$ process terminates beyond $Z = 24$, because $E_{L_1L_2M_1}$ is negative beyond this point. The $L_1L_3M_1$ process terminates beyond $Z = 30$ for the same reason. Since the $L_1L_2M_1$ rate is essentially $\frac{1}{2}$ the $L_1L_3M_1$ rate in this region, a sharp break in the s/p ratio occurs at $Z = 24$. We have scaled this out in Fig. 2 by multiplying the s/p ratio by 1.5 above $Z = 24$. The second reason for the strong s/p variation arises from the total $L_1L_{2,3}M_{2,3}$ rate which seems to increase linearly with Z .¹⁶ Thus we plot the Chen *et al.*¹⁶ results in Fig. 2, using the quantity $(s/p)Z$ (1.5 for $Z > 24$). McGuire's³¹ results do not show the drop off of the $L_1L_2M_1$ process in this region (different $E_{L_1L_{2,3}M}$ were used as discussed above); therefore McGuire's results are plotted simply as $Z(s/p)$. Both plots still have an appreciable variation over this narrow range of Z .

The experimental s/p results are equally uncertain because the $L_1L_{2,3}V$ line shape at these low kinetic energies lies on top of a large secondary electron contribution. Experimental results exist only for Ar. The results of Mehlhorn³³ obtained from the s/p area ratios in the $L_1L_{2,3}V$ line shape are indicated with a large uncertainty to emphasize the background problem. McGuire analyzed the Ar $L_{2,3}M-M^3$ satellite structure at higher kinetic energies.³⁴ The initial state of these satellites arises from both the $L_1L_{2,3}M$ Auger process as well as from initial-state shakeoff. Based on this analysis McGuire concluded the s/p ratio for Ar is ~ 0.5 , a factor of 2 less than his theoretical estimate and a factor of 2 greater than Mehlhorn's experimental estimate.³⁴ Our best estimate for Si is then obtained using an extrapolation [$Z(s/p) \approx 30$] of the theoretical results of Chen *et al.*,¹⁶ but scaled by $\frac{9}{23}$ to match the experimental result for Ar, i.e., $(s/p)_{Si} \approx (\frac{30}{14}) \times (\frac{9}{23}) \approx 0.8$. This result is indicated in Table I along with an estimated large uncertainty.

Similar experimental and theoretical ss/pp and sp/pp plots for the $L_{2,3}MM$ and KMM processes have been reported elsewhere.^{1,17} Whereas the theoretical and experimental results are in excellent agreement for the KL_1M and $KL_{2,3}M$ line shapes, large discrepancies are found between the one-electron theoretical results and the experimental results for the $L_{2,3}MM$ and KMM processes.^{1,17} This has been attributed to the larger final-state electron correlation effects that exist when two holes are in the small shell. Indeed, theoretical results which included electron correlation effects [such as from configuration interaction (CI) calculations] were found to agree nicely with experiment.³⁵⁻³⁸ Furthermore the one-electron theoretical results for different Z (Refs. 16, 39, and 40)

TABLE I. Comparison of the atomic Auger intensity ratios.

Line shape	s/p or sl/pp	Intensity ratio ^a	Intensity ratio ^b
KL_1V	s/p	0.79	0.75 ± 0.1
$KL_{2,3}V$	s/p	0.23	0.3 ± 0.1
$L_1L_{2,3}V$	s/p	0.64	0.8 ± 0.4
$L_{2,3}VV$	ss/pp	0.01 (0.0007) ^c	0.025 ± 0.001
	sp/pp	0.10 (0.073) ^c	0.38 ± 0.02
KVV	ss/pp	0.10	0.15 ± 0.02
	sp/pp	0.48	0.46 ± 0.02

^aIntensity ratios (e.g., A_{ccs}/A_{ccp}) obtained from the fit of Eqs. (4) and (5) to the experimental line shapes.

^bIntensity ratios (e.g., A_{ccs}/A_{ccp}) from Fig. 2 and Refs. 1 and 17 as discussed in the text.

^cResults of Kunjunny *et al.* (Ref. 8) obtained without the inclusion of the R factors in Eq. (5).

could be scaled (requiring factors from 0.6 to 2) by a constant factor to give excellent agreement with experiment; this indicates a constant correlation effect.¹ The optimal intensity ratios obtained from extrapolation of these plots are given in Table I.

C. Screened and unscreened valence DOS

The CVV line shapes should reflect the final DOS in the absence of a core hole, consistent with the FS rule and Eq. (5). If the final-state holes completely delocalize,^{1,4-9} the final state is accurately represented by the ground DOS. We shall use the DOS calculated by Papaconstantopoulos and Economou¹⁴ utilizing the Slater-Koster parametrized tight-binding Hamiltonian, constructed using four orthogonal orbitals per site. These can be compared to the KV and $L_{2,3}V$ x-ray emission spectra (XES),⁴¹ which reflect the ground state p and s DOS, respectively, consistent with the FS rule.²³⁻²⁶ This comparison is shown in Figs. 3(a) and 4(a) where the occupied theoretical DOS have been broadened with a gaussian of full width at half maximum (FWHM) equal to 1.5 eV to account for the experimental resolution and core-hole lifetime broadening.

The CCV line shapes, on the other hand, reflect a screened DOS, local to the core hole. The Hamiltonian which describes the screened core hole can be approximated within the tight-binding approximation (TBA),¹⁵

$$H = \sum_m |m\rangle \epsilon_0 \langle m| + V \sum_{n,m} |n\rangle \langle m| - |l\rangle \epsilon \langle l|, \quad (13)$$

where each state $|m\rangle$ is an atomiclike orbital centered at site m which form a regular lattice and ϵ_0 is the energy of an electron at site l in the absence of V . V is the hopping amplitude for transfer of an electron from one site to another. The core hole is located at site l and introduces the perturbation $-|l\rangle \epsilon \langle l|$ such that the diagonal matrix element $\langle l|H|l\rangle$ equals $\epsilon_0 - \epsilon$. The DOS at the core-hole site, $N_l(E)$, can be obtained from the DOS at the remaining sites, $N_m(E)$, utilizing Green's-function techniques,¹⁵ which give

$$N_l(E) = \frac{N_m(E)}{[1 - \epsilon I(E)]^2 + \epsilon^2 \pi^2 N_m^2(E)}. \quad (14)$$

Here $I(E)$ is the Hilbert transform of the DOS,

$$I(E) = \int [N_m(E')/(E - E')] dE'. \quad (15)$$

Equations (14) and (15) are remarkably similar to Eqs. (8) and (9) showing that the polarization parameter ϵ plays the same role in the distortion of N_m as the Coulomb repulsion U plays in the distortion of $N_l(E) * N_l(E)$.

The distortion to $N_l(E)$ from $N_m(E)$ can be seen in Fig. 5 for ϵ equal to 0, 2, 4, and 6 eV utilizing both the s and p DOS as determined by Papaconstantopoulos and Economou.¹⁴ The sum of $N_l(E)$ up to the Fermi level, ϵ_F , is indicated also; the integral of $N_l(E)$ over the occupied and unoccupied DOS of course remains constant. The distortion reflects the polarization of charge (i.e., to the core-hole site in the bonding band orbitals and away in the

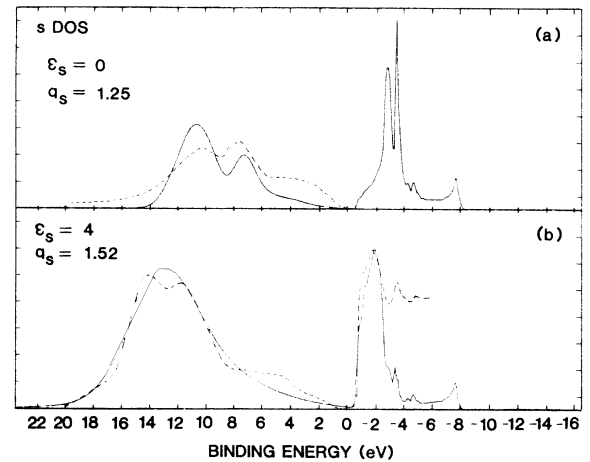


FIG. 3. (a) Comparison of the s DOS for Si as obtained from the Slater-Koster parametrized tight-binding Hamiltonian (Ref. 14) and Gaussian broadened by 1.5 eV (solid line) with that indicated from the $L_{2,3}V$ XES spectrum (dashed line) (Ref. 41). (b) Comparison of the core-hole screened s DOS, as obtained from Eq. (14) using the theoretical DOS as in (a) and a central potential of $\epsilon_s = 4$ eV (solid line), with that indicated from the $L_{2,3}L_{2,3}$ - $L_{2,3}V$ XES (Ref. 43) spectrum, and the $L_{2,3}$ absorption spectrum (dashed line) (Ref. 48). The occupied theoretical DOS has been broadened by 5.5 eV. The unoccupied DOS has not been broadened.

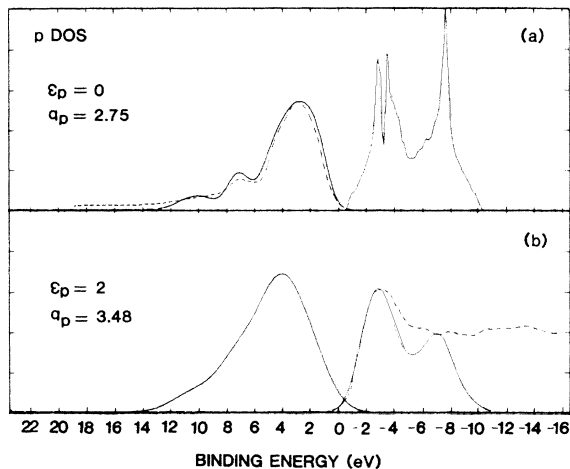


FIG. 4. (a) Comparison of the theoretical p DOS obtained as in Fig. 3(a) (solid line) with that indicated by the KV XES spectrum (dashed line) (Ref. 41). (b) Comparison of the core-hole screened p DOS, obtained as in Fig. 3(b) and using a value of $\epsilon_p = 2$ eV (solid line), with the K absorption spectrum (dashed line) (Ref. 48). The occupied DOS has been broadened by 3 eV, the unoccupied by 1.7 eV.

antibonding band orbitals). The increase in the occupied DOS as ϵ increases reflects the net charge transfer to the core-hole site. Note, also, that the appearance of an increasingly localized state below the valence band and an excitoniclike state beginning to appear at the bottom of the conduction band for the larger ϵ values in the s DOS.

The polarization parameter ϵ can be related to the fully

screened and relaxed electron core-hole attraction. Its value for Si is not known accurately. We can estimate this value for a $2p$ core hole in the free atom from the $L_1L_{2,3}M$ electron energies calculated by Chen *et al.*³² and the expression

$$E_{L_1L_{2,3}M} = E_{L_1} - E_{L_{2,3}} - E_M - \epsilon. \quad (16)$$

The XPS atomic binding energies E_{L_1} , $E_{L_{2,3}}$, and E_M are well known experimentally giving $\epsilon_s = 10$ eV and $\epsilon_p = 6.5$ eV. The larger ϵ_s value compared with ϵ_p reflects the deeper penetration of the $3s$ electrons into the core region where they experience less screening of the core hole from the other valence electrons. The polarization energies in the solid should of course be smaller, due to extra-atomic relaxation and screening.⁴²

The value of ϵ_s for a $2p$ core hole in the solid can be obtained by comparison of Fig. 5 with the Si $L_{2,3}L_{2,3}-L_{2,3}V$ XES data.⁴³ The $L_{2,3}^2-L_{2,3}V$ line shape reflects the screened s DOS, consistent with the FS rule, and selection rules for the x-ray emission process. The best fit to the XES line shape is obtained with an ϵ_s value of 4 eV. This comparison is given in Fig. 3(b) where the occupied theoretical DOS has been folded with a Gaussian of 5.5 eV. This width reflects a component of 1–2 eV for experimental resolution and lifetime broadening, and a component of 3–4 eV to account for the exchange correlation effects between the core- and localized-valence holes⁹ and other resonant broadening mechanisms.⁴⁴ It is expected that such exchange correlation effects could broaden the DOS by some fraction of the central-cell potential ϵ_s , and hence be of the order of 3–4 eV.

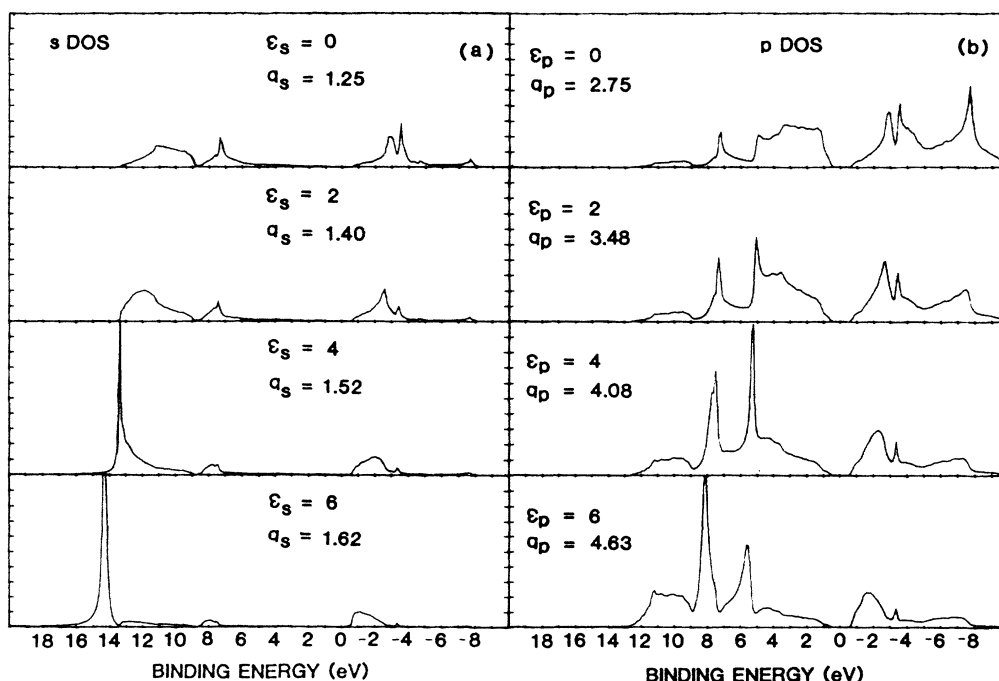


FIG. 5. (a) Comparison of the core-hole screened s DOS for Si as obtained from Eq. (14) utilizing the theoretical Slater-Koster parametrized tight-binding Hamiltonian and the central-cell potentials of $\epsilon_s = 0, 2, 4,$ and 6 eV. (b) Comparison of the core-hole screened p DOS obtained as in (a).

A similar determination of ϵ_p for a $2p$ core hole in the solid is not possible, since we are not aware of any $KL_{2,3}\text{-}L_{2,3}V$ XES data, although we know of no reason why it would not be measurable. A reasonable value of ϵ_p can be obtained, however, by comparison of Fig. 5(b) with the KL_1V and $KL_{2,3}V$ Auger data. This comparison suggests that the principal peak in the $2p$ DOS shifts to a 2 eV higher binding energy (BE) in the presence of a core hole. Thus, a value of $\epsilon_p = 2$ eV is indicated. The DOS obtained from Eq. (14) is shown in Fig. 4(b) after Gaussian broadening by 3 eV. The 3 eV may again be divided into a component of 1–2 eV from experimental resolution and lifetime broadening and a component of 1–2 eV from core-valence exchange correlation, etc.; the latter component is smaller than in the s DOS because ϵ_p is less than ϵ_s .

The values of ϵ_s and ϵ_p for $1s$ and $2s$ core holes cannot be obtained independently, since obviously no XES or AES data exist with a $1s$ or $2s$ final state. It can be assumed, however, that the central-cell polarization potential ϵ is the same for all of the core holes within the equivalent cores (EC) (Ref. 45) or the optical alchemy approximation.⁴⁶ These approximations indicate that an atom with a core hole is equivalent to the transmutation of the excited atom into an atom with a nuclear charge $Z + 1$, provided that the hole occupies a smaller radius than the electrons in the valence and conduction bands.

Comparison of the binding energy of the Si $2p$ core exciton with that of the P (Si $Z + 1$ transmutant) substitutional donor level, however, suggests that there may in fact be a difference between the $1s$ and $2p$ core holes. The P in Si donor level is of the Wannier type having a 45 meV binding energy⁴⁷ and according to the EC approximation should closely approximate the $1s$ core exciton in Si. The Si $2p$ core exciton appears to be of the deeper Frenkel type with an experimental binding energy of 0.15 to 0.8 eV.^{48–51} Although still under discussion,⁵⁰ recent resonant photoemission data on Si(111) near the $2p$ core excitation threshold strongly suggest that the excitoniclike state is sufficiently long lived for the excited electron to participate in the Auger decay or be a spectator to it (i.e., produce resonant photoemission or satellite emission).

Recent calculations by Hjalmarsen *et al.*,⁵¹ utilizing the central-cell TBA model such as that utilized here, predict a Wannier-type Si $2p$ core exciton level which lies 0.02 eV above the band gap. This is in reasonable agreement with our results in Fig. 5 showing an excitoniclike state appearing at the bottom of the conduction band in the s DOS. Increasing the central-cell potential will eventually cause a deep level below the conduction-band edge, but larger values of ϵ_s and ϵ_p are not indicated from a comparison of theory and experiment in the occupied DOS. Many possibilities have been discussed recently to explain the deep Si $2p$ excitonic level including intervalley scattering,⁵² screening of the core-hole self-energy by the electron orbit,⁵³ incomplete electron relaxation,⁵⁴ and surface effects.⁴⁹ It is clear that the central-cell TBA models, such as that used here which ignore these effects, as well as the long-range Coulomb interaction, cannot adequately predict the core exciton binding energy.

The Auger process samples only the occupied DOS, so

that the nature of the core exciton and the unoccupied DOS is not reflected in the Auger line shape. Nevertheless we can check the quality of our unoccupied s and p DOS in the presence of a core hole by comparison with the experimental Si $2p$ and $1s$ absorption spectra which reflect these states.⁴⁸ These comparisons are given in Figs. 3(b) and 4(b) and reveal remarkably good agreement. Note that in this case the unoccupied theoretical DOS does not require large Gaussian broadening (~ 0 eV and 1.7 eV to reflect the photon spectral width) because the resonant broadening mechanism⁴⁴ and exchange correlation effects⁹ occur only in the presence of two holes (core and valence).

It seems clear that in spite of some problem with the core exciton binding energies, we can safely assume the validity of the EC approximation and the central-cell TBA model for the occupied DOS of interest in this work (and for the overall unoccupied DOS). Comparison of the theoretical line shapes with the experimental line shapes will provide a check on this assumption.

Another check on the consistency of our screened DOS comes from the total charge transfer. Figures 3 and 4 indicate an s charge transfer of 0.27 electrons and a p charge transfer of 0.73 electrons for a total of 1.0 electron. If this result is correct, it reveals the charge transfer of a whole electron to the core hole even in a semiconductor such as Si, where one might have expected somewhat less. Another point is worth noting, Figs. 3 and 4 suggest that the s DOS suffers a much larger distortion than the p DOS; however, the p DOS brings about the larger charge transfer. The larger distortion of the s DOS was already evident from the qualitative work of Lasser and Fuggle,⁹ and indeed they suggested that as one progressed from left to right in the series Na, Mg, Al, and Si, the charge transfer shifted from mostly s -like to p -like because the s DOS are becoming increasingly filled. Our screened DOS are consistent with this conclusion.

A final check on the screened DOS can be obtained from the total dynamic relaxation energy of the Si $2p$ core level, $R_D(2p)^{\text{Si}}$, which will be dominated by the valence-atomic and extra-atomic relaxation terms, $R_D^{\text{a(val)}}(2p)$ and $R_D^{\text{ea}}(2p)$, respectively.⁵⁵ In the central-cell approximation utilized in this work, the total valence relaxation energy can be approximated from the expression

$$R_D(2p)^{\text{Si}} = 2 \int_{\text{occ}} \epsilon [N'_s(\epsilon) - N_s(\epsilon) + N'_p(\epsilon) - N_p(\epsilon)] d\epsilon. \quad (17)$$

This expression and the DOS in Figs. 3 and 4 gives $R_D(2p)^{\text{Si}}$ equal to 11.9 eV. Theoretical estimates for $R_D^{\text{a}}(2p)^{\text{Si}}$ ranging from 4.3 to 6.8 eV have been reported as summarized by Bechstedt *et al.*⁵⁵ $R_D^{\text{a(val)}}(2p)^{\text{Si}}$ can be estimated as one-half the static relaxation energy as given by Shirley,⁵⁶ i.e., $R_D^{\text{a(val)}}(2p)^{\text{Si}} \sim 7$ eV. Bechstedt gives a result as low as 2.7 eV. Thus estimates for $R_D(2p)^{\text{Si}}$ range from 7.4 to 13.8 eV. Our result is at the upper limit of this range which appears most reasonable.

IV. RESULT AND DISCUSSION

A. CCV Auger line shapes

The CCV line shapes directly reflect the screened DOS consistent with the FS rule. Figures 6–8 compare the ex-

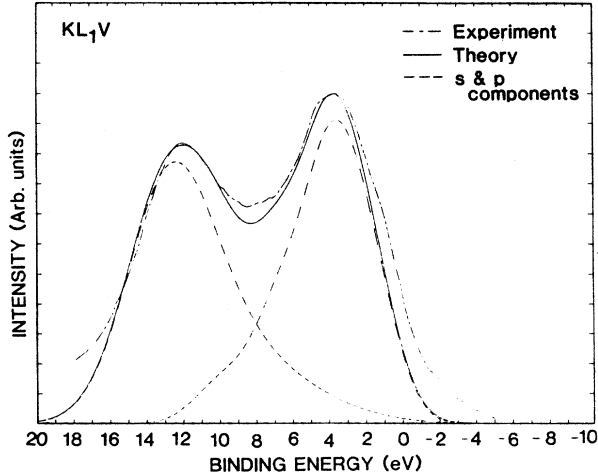


FIG. 6. Comparison of the experimental (variable dashed line) KL_1V line shape (Ref. 9) with the optimal fit of Eq. (4) (solid line), utilizing the s and p DOS exactly as shown in Figs. 3(b) and 4(b). The theoretical s and p contributions are indicated by the dashed lines. The experimental line shape has been shifted by 2.0 eV to lower binding energy to provide an optimal fit with Eq. (4).

perimental KL_1V , $KL_{2,3}V$, and $L_1L_{2,3}V$ line shapes with the optimal fit of Eq. (4). Small shifts of the experimental spectra by 2.0, 0.7, and 0.4 eV, respectively, to lower binding energy were needed to obtain optimum agreement with Eq. (4). The shifts of less than 1 eV are of the order of the error in the placement of the Fermi level.⁹ The reason for the large shift required for the KL_1V spectrum is not known, but we doubt whether it has a fundamental basis. Table I compares the approximate ratios with the empirical matrix elements. These results show excellent agreement within experimental uncertainties and provide quantitative support for the applicability of the FS rule to the CCV line shapes and the central-cell TBA model for the occupied DOS.

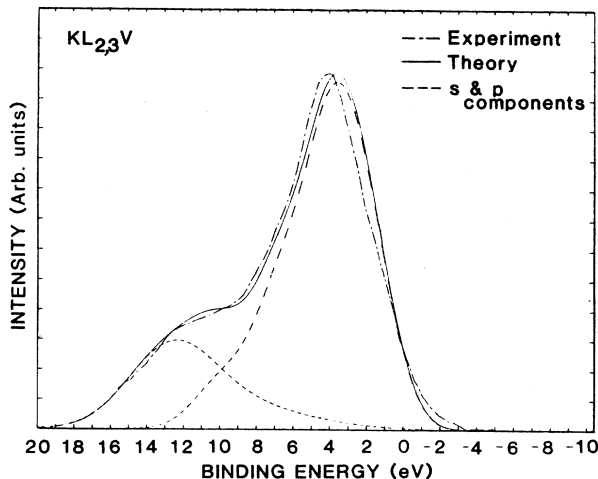


FIG. 7. Same as Fig. 6 but for the $KL_{2,3}V$ line shape (Ref. 9) which was shifted by 0.7 eV.

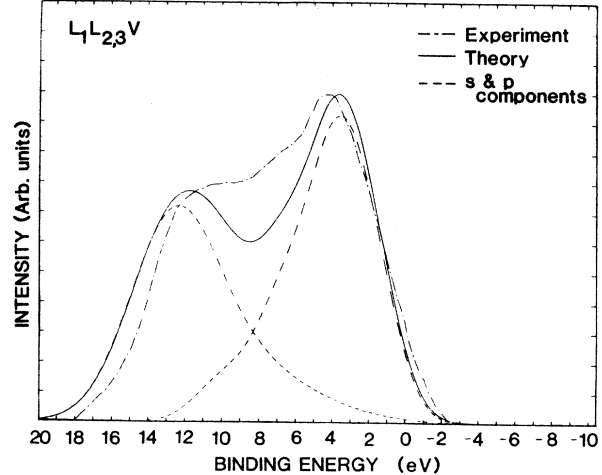


FIG. 8. Same as Fig. 6 but for the $L_1L_{2,3}V$ line shape (Ref. 3) which was shifted by 0.4 eV.

B. CVV Auger line shapes

1. $L_{2,3}VV$ line shape

The CVV line shapes should reflect a fold of the ground-state DOS consistent with our discussion in Sec. III A. Figure 9 compares the experimental $L_{2,3}VV$ line shapes with the optimal fit of Eq. (5). The $2p_{3/2}$ binding energy relative to the Fermi level is well established at 99.6 eV when referenced to the Au $4f_{7/2}$ peak assigned an energy of 84.0 eV.⁵⁷ This enables the theoretical $L_{2,3}VV$ Auger energy scale to be accurately determined. The experimental peak energy in $N(E)$ has been determined by several workers on many different Si crystal faces. Examining these results we place the best estimate at 93.0 ± 0.5 eV.^{3,5,7,57} This allows a comparison between the theoretical line shape obtained using Eq. (5), and the experimental line shape on an absolute energy scale. Figure 9 shows that with these assumptions, the peaks are not in registry and the slope near the top of the line shapes are different. Actually the onset of the two line shapes near the Fermi level are in relatively good agreement. This suggests the presence of some distortion due to final-state hole-hole correlation effects. Use of Eq. (8) applied separately to both the $N_s * N_s$, $N_s * N_p$, and $N_p * N_p$ folds and U 's of 2.3, 2.3, and 0.4 eV, respectively, provide excellent agreement with experiment. These U 's are reasonable compared with 3.5–4 eV in the σ bonds of graphite (a semimetal)⁵⁸ and ~ 0 eV on the C atom in the pp band of transition-metal carbides (conductors).⁵⁹

In Fig. 9(a), the coefficients C_{ss} , C_{sp} , and C_{pp} of Eq. (5) are optimized for the $U \neq 0$ eV distorted line shape and forced to be the same for the $U = 0$ undistorted line shape. This allows a simple visual determination of the effects of hole-hole correlation. Optimization of the C_{ij} coefficients for the undistorted ($U = 0$) folds improved the fit somewhat, but could not give a satisfactory fit to the experimental line shape as shown in Fig. 9(b).

A similar self-fold of the DOS and comparison with the

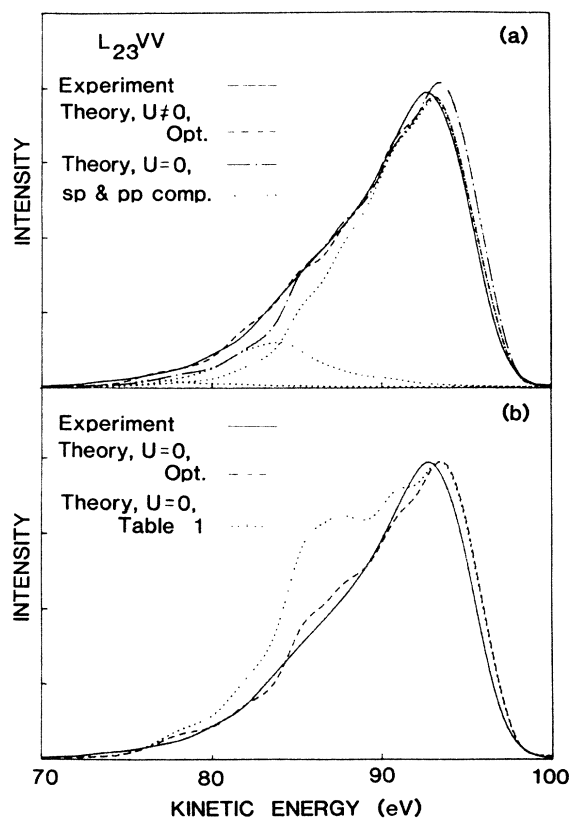


FIG. 9. (a) Comparison of the experimental $L_{2,3}VV$ line shape (Ref. 3) with the optimal fit of Eq. (5) and $U_{ss} = U_{sp} = 2.3$ and $U_{pp} = 0.4$ eV as described in the text. The theoretical line shape was Gaussian broadened by 1.5 eV consistent with Figs. 3(a) and 4(a). Also shown is the fit of Eq. (5) using $U = 0$ but with the same $C_{ll'}$ coefficients as obtained from the $U \neq 0$ fit. The theoretical sp and pp contributions are indicated by the dotted lines. (b) Comparison of the experimental $L_{2,3}VV$ line shape with the optimal fit of Eq. (5) and using $U = 0$. Also shown is a line shape using Eq. (5) and $U = 0$ but with the $C_{ll'}$ coefficients generated from the $A_{ll'}$ given in the last column of Table I.

$L_{2,3}VV$ line shape for Al shows just the opposite situation from that for Si, that is the peak in the self-fold appears further down from the Fermi level than in the experimental line shape.⁶⁰⁻⁶³ This clearly indicates that hole-hole correlation effects are much less important in Al than in Si, as one might expect for a metal. In Al, inclusion of surface effects, due to the small sampling depth of the $L_{2,3}VV$ electrons, has been suggested as a mechanism which will shift the theoretical peak back up towards the Fermi level and into registry with experiment.⁶⁰⁻⁶³ Near the surface, calculations show that the ss and sp components should be reduced, thus having the effect of increasing the relative importance of the pp component, which has its peak nearer the Fermi level.^{61,63}

Including surface effects in the self-fold of the pp DOS for Si also causes the $L_{2,3}VV$ peak to occur closer to the Fermi level,⁸ suggesting that if these effects were included, an even larger U for Si would be required to lower the peak back to its experimental position. Thus localization effects are indicated in Si; however, uncertainties in the ex-

act placement of the $L_{2,3}VV$ line shape make it impossible to determine accurately the value of U . Indeed, it should be mentioned that previous comparisons of the empirically (e.g., using the $K\beta$ XES spectrum) calculated line shapes with the experimental $L_{2,3}VV$ line shape gave good agreement in the peak positions, as well as in the slopes of $N(E)$ above the mean peak.⁴⁻⁸ Evidently, ones conclusions can easily be affected by the placement of the energy scale, and the exact nature of the calculated DOS. Our results for Si are consistent with those recently reported for graphite, Al, and other conductors and insulators as discussed above, but localization effects in the Si $L_{2,3}VV$ line shape cannot be positively identified under these circumstances.

Although excellent agreement between theory and experiment is found in Fig. 9, Table I reveals that the coefficient ratios from the best $U \neq 0$ eV fit does not at all agree with the empirical matrix element ratios. This arises even though the $L_{2,3}VV$ matrix element ratios are well established. The apparent near lack of ss and sp contributions in the $L_{2,3}VV$ line shape indicated in Table I and Fig. 9 is well known, indeed we include previous results of Kunjunny *et al.*⁸ in Table I for comparison. The R factors have not been included in the work of Kunjunny *et al.*⁸ The R factors improve the situation, but by less than 10%.

The substantial decrease of the ss and sp contributions suggests that for some reason major parts of the s DOS is not sampled by the Auger process. Jennison⁶ has shown that because the interatomic ss overlap is significantly larger than the pp overlap, the s DOS contributes a significantly greater portion to the bonding charge. He further indicates that the bonding charge is not sampled by the Auger process. The Si $3s$ orbitals are known to be relaxed and radially extended in the solid relative to that in the free atom⁶⁴ and this does increase the interatomic ss overlap in the ground state. However, in the presence of a core hole, the $3s$ orbitals are expected to radially contract back to what they were in the free atom, and according to the FS rule the ll' relative intensities are dictated by the screened core-hole initial state. Furthermore, previous examination of this bonding charge contribution on the Auger line shapes of equally covalent systems, such as NO_3^- , PO_4^{3-} , SO_4^{2-} ,^{65,66} and Pd_4Si ,^{67,68} did not reveal a significant effect. Thus we do not believe that the bonding charge concept is the sole mechanism for the reduced ss and sp components, although it could be partially responsible.

We proposed previously⁶⁹ that the lack of the ss and sp contributions in both line shapes could arise from final-state shakeoff, which is introduced because of the atomic relaxation of the Si $3s$ orbitals mentioned above. The large difference in the radial extent of the $3s$ orbital in the screened and unscreened state means a large contribution [i.e., the Si f' contributions in Eq. (3)] must be projected or orthogonalized out of the s DOS when utilizing the orthogonalized FS rule. This "projected out" portion of the s DOS must also be projected out of the normal Auger line shape and is redistributed at lower energy, over a wide energy range, as intrinsic loss. This intrinsic loss contribution if present cannot be distinguished from the normal

extrinsic loss and so it is taken out as background. A large final-state shakeoff or intrinsic loss contribution indicates a breakdown in the FS rule,² Eq. (1), but it arises naturally in the orthogonalized FS rule if the f' terms are included in Eq. (3). We have indicated previously (Sec. III A) that the orthogonalized FS rule cannot be easily applied quantitatively, and hence it is not attempted here.

2. KVV line shape

Our primary motivation for measuring the KVV line shape was to determine if the ss and sp contributions are extremely small here as well. The extremely weak intensity of the KVV line shape and the poor energy resolution of the CMA at this high KVV kinetic energy prevented us from accurately determining the line shape. Nevertheless, it is clear from the comparison of Figs. 9 and 10 that the LVV and KVV line shapes are qualitatively different.

The intensity in the experimental KVV line shape immediately above the main peak is probably due to an autoionization process $K\bar{E}-V$, where \bar{E} denotes an "exciton-like" electron in the conduction band as mentioned in Sec. III C. This autoionization contribution is larger in the KVV line shape than in the LVV line shape probably because of the shorter lifetime of the K core level. Some evidence also exists in the KL_V line shapes (especially in the $KL_{1,V}$ line shape) for contributions from this process. The small features between 1850 and 880 eV are attributed to $KL_{2,3}-L_{2,3}VV$ shakeup satellites similar to those recently reported above the Mg $KL_{2,3}V$ line shape.⁷⁰ The structure between 1770 and 1790 eV in Fig. 1 could arise from similar satellites above the Si $KL_{2,3}V$ line shape.

A relatively large intensity also exists near the bottom of the line shape, around 1812 eV. Also, this intensity cannot come from the normal line shape since it extends down to 1804 eV, well below the ~ 1811 -eV minimum en-

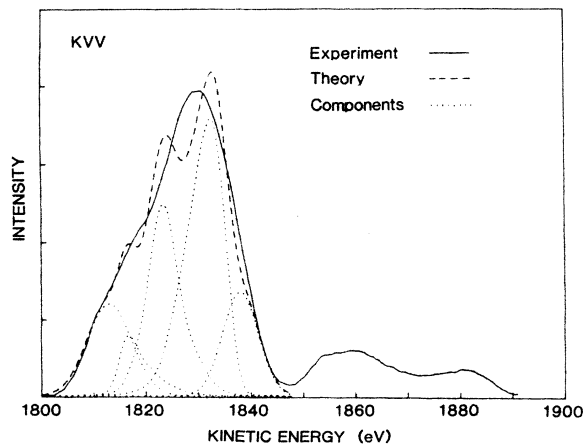


FIG. 10. Comparison of the experimental KVV line shape from Fig. 1 with the optimal fit of Eq. (5) using the same U 's as in Fig. 9 for the LVV line shape, plus Gaussians at 1813 and 1838 eV with widths of 8 and 7 eV, which account for the plasmon and excitonic contributions as described in the text. The resultant plasmon, ss , sp , and pp Auger, and excitonic contributions (in order of increasing energy) are indicated by the dotted lines. The theory was broadened by 3 eV.

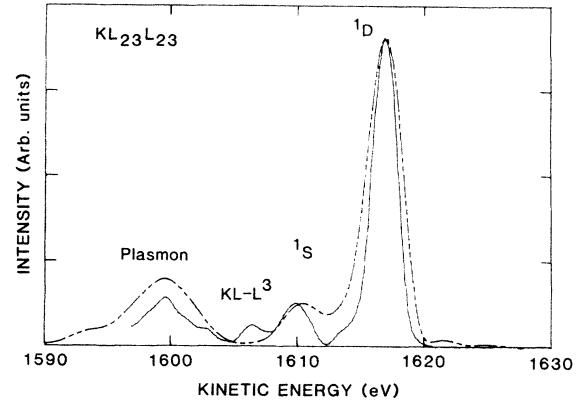


FIG. 11. Comparison of the $KL_{2,3}L_{2,3}$ line shape as obtained in this work (dashed line) (Sec. II) with that obtained by Cazaux and Minh Duc (Ref. 22) (solid line) using bremsstrahlung radiation. A background has been subtracted and losses deconvoluted as described in the text. The $1D$, $1S$, plasmon loss, and $KL-L^3$ shakeoff peaks are indicated.

ergy expected for the normal line shape [i.e., below $E_c - 2\Gamma_{bb} = 1839 - 2(14) = 1811$ eV]. A possible explanation for this intensity is that dynamic screening of the valence holes could be important. Recently, Cini has extended his hole correlation theory, as contained in Eq. (8), to include electron screening from the remaining amount of electrons in the valence bands.⁷¹ Whereas Eq. (8) incorporates the "static" screening by utilizing an effective U , the new theory begins with the unscreened U , and includes the dynamic screening directly in the calculations. Unfortunately, this is much more difficult to apply numerically to our DOS, but Cini has shown that for a model DOS, the effect of the dynamic screening is to introduce intrinsic plasmon-loss contributions at the bottom of the line shape. Earlier work has indeed shown that an intrinsic plasmon-loss peak is expected below the LVV spectrum in Al.⁶³

It is important to realize that the losses mentioned above are intrinsic to the Auger line shape. This is in contrast to the extrinsic losses resulting from inelastic collisions that the Auger electrons suffer on their way out of the solid. The extrinsic losses should be removed from the Auger line shape in the deconvolution procedure, although there is some question as to whether Auger and primary electrons suffer similar loss processes.⁷² The energy separation in Fig. 10 between the "intrinsic loss contribution" and the main peak is reasonably consistent with the known bulk plasmon energy of 17 eV.²² Thus, all or some of the intensity below 1820 eV could result from unremoved extrinsic plasmon losses, a definite possibility considering the experimental problems with the KVV line shape.

We believe that at least some of the intensity around 1810 eV arises from intrinsic losses. We ask the question, why are similar intrinsic loss contributions apparently not present in the Si LVV line shape? The extreme surface sensitivity of the ~ 90 -eV LVV electrons could cause a reduction in the intrinsic plasmon component, but this is only speculation.

The large difference between the *KVV* and *LVV* line shapes could come entirely from the additional plasmon and excitoniclike contributions in the *KVV* line shape, or it could mean that the total *ss* and *sp* contributions indeed are present in the *KVV* line shape. To test this, we have applied Eq. (5) to the experimental *KVV* line shape assuming the same *U*'s as determined for the *LVV* line shape, and including Gaussians at 1813 (17 eV below the major Auger peak) and 1839 ± 1 eV (near the Fermi level) with widths of 8 and 7 eV for the plasmon and excitonic contributions. The relative Auger, plasmon, and excitonic contributions are varied for best agreement with the experimental line shape. Relatively good agreement is found as shown in Fig. 10. Table I indicates that the *ss* and *sp* intensity ratios are in this case much closer to the expected intensity ratios than found for the *LVV* line shape. It should be acknowledged here that the relative *ss* and *sp* contributions can be varied somewhat by changing the plasmon intensity. Furthermore, there is uncertainty in the *KVV* line shape because of the poor resolution of the CMA at the high *KVV* energy. Thus it is impossible to definitely establish the magnitude of the *ss* and *sp* contributions in the *KVV* line shape, but they are clearly larger and closer to the theoretical predictions of Table I compared with that found for the *LVV* line shape. The poor experimental resolution probably also accounts for the reduced structure in the experimental line shape compared with that found in the theoretical line shape.

3. Comparison with other systems

Data for the neighboring elements Mg, Al, and P are equally uncertain. Recently Davies *et al.*⁷⁰ reported the *KVV* line shape for Mg and compared it with the previously reported *LVV* line shape.⁷² They concluded that the small differences between the line shapes could be accounted for by the different atomic intensity ratios between the *LVV* and *KVV* processes as shown in Table I. However, both the *KVV* and *LVV* line shapes (in this case the *LVV* does have a plasmon loss but apparently still smaller than the *KVV*) have plasmon losses just below the main line shapes, and uncertainties in removing this intensity exist in both cases so that the presence of intrinsic losses have not definitely been established.^{70,72} Furthermore, the *sp* and *pp* spectral line shapes in Mg are similar, making it rather difficult to determine their exact relative contributions by the curve-fitting procedure of Davies *et al.*, a procedure very similar to that indicated by Eq. (5).

The more important question for Mg concerns the overall *s* to *p* charge ratio. Davies *et al.*⁷⁰ concluded from the procedure above that the core-hole initial state had the ratio *s:p* = 1:1.9. For the ground state of Mg, theoretical calculations by Gupta and Freeman⁷³ indicated a ratio of 1:0.85 for the region of the muffin tin used in their band calculations. Citrin *et al.*⁷³ obtained an *s:p* ratio of 1:0.11 when projecting out the orbital character of their pseudopotential wave function using a cutoff radius of *R* = 1 a.u., and a ratio of 1:1.1 when using a cutoff radius of *R* = 3 a.u. The latter result is clearly more comparable with the results of Gupta and Freeman. Finally,

Jennison utilized Δ SCF excited atom model calculations and comparison with XPS and Auger Mg atom-metal-core level energy shifts to conclude that the charge configurations are $3s^1 3p^1$, $3s^2 3p^1$, and $3s^2 3p^2$ for the ground state, and one and two core-hole states, respectively.⁷⁰

Thus, all of the calculations appear to be consistent, and on first sight the Mg *CVV* line shapes appear to be consistent with the calculations, as suggested by Davies *et al.*⁷⁰ However, several unsettling points need to be raised. First Davies *et al.*⁷⁰ argue that the *R* = 1 a.u. cutoff result of Citrin *et al.* is more appropriate for initial core-level spectroscopies such as XES or the Auger process, with the *R* = 3 a.u. cutoff result more appropriate for photoemission and comparison with "atomic" calculations. If the Auger line shape should reflect the *R* = 1 a.u. cutoff ratio, a much larger *s:p* ratio (somewhere between 2:0.1 and 1:1.1 depending on whether the screening charge is total *s* or *p* like) should be reflected in the *CVV* line shape. Second, in contrast to the assumptions of Davies *et al.*,⁷⁰ the calculations of Citrin *et al.* indicate that the extended charge or "bonding" charge is mostly *p*-like, not *s*-like. Thus, if the bonding charge concept, utilized by Jennison to explain the Si *LVV* line shape, is also acting for Mg, it should have the opposite effect in the Mg *CVV* line shape, i.e., reduce the relative *pp* component. As indicated above, we believe that the bonding charge concept is not critical to the line shape since the *CVV* line shapes reflect the *s:p* charge ratio of the initial screened core-hole state, where the bonding charge should be strongly diminished whether it was *s*- or *p*-like in the ground state. Finally, the atomiclike intensity ratios (A_{css}/A_{cpp} and A_{csp}/A_{cpp} defined in Sec. III B) utilized by Davies *et al.*⁷⁰ were $1.5E-5$ and 0.22, respectively, for the *LVV*, and 0.024 and 0.23 for the *KVV* line shape. The A_{csp}/A_{cpp} values above for both the *LVV* and *KVV* line shapes are approximately one-half the empirical ones tabulated in Table I. This factor of 2 may arise from a different definition of the $N_s(E) * N_p(E)$ fold, but their Eq. (1) in Ref. 70 should then show a factor of 2 in front of their *sp* term. The A_{css}/A_{cpp} values are very much smaller (factors of $6E-4$ and 0.16 for the *LVV* and *KVV*, respectively). These differences were discussed in Sec. III B, and arise from the lack of correlation in the one-electron calculations of Davies *et al.*⁷⁰ All three points above suggest that the *ss* and *sp* contributions relative to the *pp* should be considerably larger than that found by Davies *et al.*⁷⁰ in the *LVV* and *KVV* line shapes, consistent with that discussed for the Si *LVV* line shapes above. However, the problems with the curve-fitting procedure for Mg as stated above, make it impossible to positively conclude much about the *s:p* charge ratio reflected in the *CVV* Auger line shapes for Mg.

Fortunately, the problems discussed above for Mg decrease as one proceeds to the right in the Periodic Table. This is because the *s* and *p* charge populations become more balanced and the *sp* and *pp* spectral line shapes become increasingly different. Interpretations of the *LVV* line shape for Al and P also indicate sharp reductions in the *ss* and *sp* contributions.^{61-63,74} The *KVV* line shapes for Al and P to our knowledge have not been reported.

4. Surface effects versus final-state shakeoff

If the *ss* and *sp* contributions are fully reflected in the *KVV* line shape, but not in the *LVV* line shapes of these four elemental solids, then final-state shakeoff is most likely not the cause of the *ss* and *sp* reductions in the *LVV* line shapes, since final-state shakeoff is expected to be equally active in both the *LVV* and *KVV* line shapes.⁷⁵ In this case, one could speculate that the differences in mean free paths of the high energy *KVV* electrons versus the small energy of the *LVV* electrons causes the differences. It has been proposed that the dangling bonds at the surface in Si are primarily *p*-like with the backbonds of the surface Si atoms primarily *sp*²-like.⁷⁶ An extremely short sampling depth of the *LVV* Auger process (i.e., sampling primarily the *p*-like dangling bonds and only part of the *sp*² backbonds) would then explain the predominance of *pp*-like character in the *LVV* line shape. Surface effects in the *LVV* line shapes have been theoretically studied previously, e.g., in Si in the original work by Feibelman *et al.*⁴ and more recently by Kunjunny and Ferry.⁸ These calculations do indicate that surface effects add intensity to the line shape in the region 85–95 eV, but inclusion of these surface effects does not solve the problem; indeed Feibelman's work lead to the discovery of this problem. Nevertheless, changes in the Si *LVV* experimental line shape upon chemisorption of O₂ or H₂O, or upon Ar sputtering, which is expected to tie off the surface dangling bonds or at least disrupt the Si surface structure, indicate relatively sharp reductions in the intensity around 85–95 eV compared to that below 85 eV.^{77,78} Recent cluster calculations on Si₅H₁₂ and Si₅ (Ref. 79) also show that H on the "surface" reduces the *ss* and *sp* contributions to the *LVV* line shape, and H is known to always be present in Si.⁸⁰ Calculations on Al metal also shows that the surface layers have more *p*-like character than the bulk, and indeed this has been proposed previously to explain the reduction of the *ss* and *sp* components in the Al *LVV* line shape.^{61–63} Thus we cannot rule out surface effects as a cause for the reduction in the *ss* and *sp* components in the *CVV* line shapes.

If both the *KVV* and *LVV* line shapes have reduced *ss* and *sp* components, as might be suggested for Mg, and perhaps may also be the case for Si, Al, and P, then we propose final-state shakeoff as a primary cause as explained above. These elemental solids would then provide the first instance to our knowledge where final-state shakeoff causes large changes in the Auger spectral line shape. The total Auger integrated intensity should also reflect this loss in intensity. However, a quantitative determination of the experimental Auger intensity is difficult; a determination of the shakeoff in this manner would require an accurate knowledge of the excitation cross section, the mean free path, and a host of other parameters.⁸¹ A comparison of the relative total S *L*_{2,3}*VV* Auger intensity from Ag₂S and Ag₂SO₄ has been utilized recently to indicate a large final-state shakeoff contribution arising from atomic 3*d* orbital relaxation in Ag₂SO₄.⁸² The diffuse S 3*d* orbitals are not occupied in Ag₂S, so that the intrinsic loss process does not occur in Ag₂S. Final-state shakeoff is difficult to observe even in

the gas phase because it is so difficult to distinguish the intrinsic and extrinsic loss processes; however, final-state shakeup, which can produce satellite peaks in the gas-phase spectrum, has been observed recently in the Auger line shape of atomic Mg.⁸³

Initial-state shakeoff, arising from ionization of the initial core electron, does not cause loss of intensity but rather shifts intensity throughout the normal Auger line shape. In the gas phase, this is seen as additional satellite peaks; they are very prevalent (up to 30% or even more of the total intensity) in most atomic Auger spectra [e.g., in Ar (Ref. 34), Na (Refs. 84 and 85), and Mg (Refs. 86 and 87)]. In the solid, this is seen as additional intensity somewhat shifted from the parent lines but rarely individually resolved from the parent intensity.⁶⁶ In general, one can expect approximately the same amount of final-state shake, as initial-state shake since in each case the probability for shake, *P_s*, can be related to the square of the overlap between the core-hole screened, *ψ'*, and unscreened, *ψ*, many-electron wave functions, i.e., $P_s = 1 - \langle \psi | \psi' \rangle^2$.⁸⁸ In the sudden approximation it makes no difference whether *ψ* or *ψ'* is the initial state. Recent experimental and theoretical studies⁸⁹ of the transition from adiabatic to sudden excitation indicates the sudden approximation is valid at surprisingly low energies, indicating it may be reasonably valid for the *CVV* Auger processes of Si. The initial-state shakeoff process may be aborted in the covalent systems if the valence and core holes do not remain localized. This is expected to occur in Si for valence-state shakeoff.¹ Thus little initial-state shakeoff is seen or expected in the Si *CVV* line shapes only final-state shakeoff is possible.

5. Summary of *CVV* line shapes

In summary, final-state shakeoff and intrinsic plasmon loss are both intrinsic to the Auger process and both result from a screening response by the remaining valence electrons. Final-state shakeoff results in a loss of Auger intensity (i.e., it is removed as background), intrinsic plasmon loss shifts Auger intensity down into a plasmon peak which is difficult to distinguish from extrinsic plasmon loss (i.e., the extrinsic and intrinsic contributions may or may not be removed in the deconvolution process). Under these conditions it is impossible to prove the existence of either process.

Further, the existence of surface effects is also difficult to prove. Further work is required on these *CVV* line shapes to establish the role of these processes. However, based on all of the present *KVV* and *LVV* data for Si, Al, Mg, and P, we currently think that intrinsic plasmon-loss effects are important in the *KVV* line shapes, and surface effects play a large role in the *LVV* line shapes. Furthermore, final-state hole correlation effects are present in both line shapes, particularly in the *ss* and *sp* components of the *CVV* line shapes.

C. CCC Auger line shapes

We examine only the *KL*_{2,3}*L*_{2,3} Auger line shape of the various possible CCC line shapes. It obviously does not reflect the valence DOS, but screening effects are visible.

TABLE II. Comparison of $KL_{2,3}L_{2,3}$ spectral features in Na, Mg, Al, P, and Si. Results in parentheses correspond to theoretical results. ND represents not determinable because of interference by other peaks.

Parameter	Na ^a	Mg ^b	Al ^c	Si ^d	P ^e
E_B (eV)	5.8±0.05	10.6±0.2	15.5±0.2	17.2±1	19.4±0.5
$I_B/I(^1D)$	0.65±0.05	0.84±0.03	0.82±0.02	0.33±0.07	0.48±0.05
$\Delta E(^1D-^1S)$ (eV)	4.5±0.1	5.4±0.04 (6.0) ^f	6.1±0.4 (6.9) ^g	6.9±0.1	5.7±0.6 (6.9) ^h
$I(^1S)/I(^1D)$	ND (0.124) ⁱ	0.2±0.1 0.153±0.03 ^j	0.2±0.1	0.16±0.01	0.11±0.02 (0.12) ^k
ΔE_{KL-L^3} (eV)	-7.5±0.1 (-13.2) ^l	-9±1 (-12.6) ^l	-9±1 (-14.1) ^l	-10.5±0.1 (-17.5) ^l	not observed
$I(SO)/I(^1D)$	0.09±0.01 (0.152) ^m	ND (0.108) ^m	ND (0.083) ^m	0.05±0.01 (0.065) ^m	not observed (0.049) ^m
$KLL(^1D)$ (eV)	994.3 ±0.3	1185.9±0.2	1393.2±0.2	1616.5±0.2 ⁿ	1857.3±0.2

^aReference 90.

^bReference 91.

^cReference 94.

^dReference 22 and this work.

^eReference 95.

^fReference 98.

^gReference 99.

^hReference 95.

ⁱReference 90.

^jReference 87.

^kReference 100.

^lDetermined from Eqs. (18)–(20) as discussed in text.

^mReference 88.

ⁿReference 101.

The $KL_{2,3}L_{2,3}$ line shape is interpreted in the context of similar interpretations of this line shape for Na,⁹⁰ Mg,^{91–93} and Al (Ref. 94) metals, and for P,⁹⁵ an insulator. These flank Si in the Periodic Table and provide an ideal series for comparison. However, Si is the only semiconductor in this series and might have different screening properties that could be reflected in the $KL_{2,3}L_{2,3}$ line shape.

Table II contains a comparison of the intensity and energy of various features in the line shape relative to the main 1D peak. All five line shapes show a bulk plasmon-loss peak with the relative intensity of Si and P about $\frac{1}{2}$ those of the three metals, probably reflecting the loss of free-electron character in Si and P. The bulk plasmon loss energy, E_B , increases by almost 5 eV with each increase in Z . On the other hand, the 1S and shakeoff peak energy shifts are relatively constant. This causes the KLL spectra to significantly change in appearance as the plasmon-loss peak sweeps through the 1S and shakeoff peaks with increasing Z . The shakeoff peak at -7 to -10 eV is clearly resolved in the Na data and has been interpreted as due to the $KL-LL^2$ processes.⁹⁰ These peaks are visible in the published Mg and Al data; however, they are not specifically mentioned by van Attekum and Trooster,^{91,94} and their intensity cannot be quantitatively determined because of interference with the plasmon peaks. It is not visible in P.⁹⁵ In Fig. 11 for Si, a similar shakeoff contribution is visible in the data of Cazaux and Minh Duc²² (it is also clearly visible in the data of Taylor⁵⁷ not shown in Fig. 10). It is not resolved in our data, although it may be present around 1604 eV.

The $KL-LL^2$ shakeoff contribution arises from initial-state shakeoff. The KL holes do not delocalize because in this case both holes are corelike (KM holes do delocalize before the Auger process and hence do not produce satellites in the solid¹). The probability for $L_1+L_2+L_3$ shakeoff as a result of β decay has been estimated by

Carlson *et al.*⁸⁸ utilizing Hartree-Fock atomic wave functions and the sudden approximation. This theoretical probability varies linearly with Z as indicated in Table II. An analysis of atomic Auger data for atomic Na (Refs. 84–86) and Mg (Refs. 87 and 88) indicates the shakeoff probability is in remarkably good agreement with these theoretical results. Data from covalent molecular gases indicate the molecular environment does not alter significantly the shakeoff probability (as opposed to the shakeup probability that does vary).⁹⁶ Although further work is required before one can draw any firm conclusions about shakeoff probabilities in these covalent solids, the relative shakeoff probabilities are in reasonable agreement with those predicted by the theory.

The energy shift $E_{KL-L^3}-E_{KLL}$ can be estimated from the expression^{97,65}

$$\begin{aligned} \Delta E_{KL-L^3} &= E_{KL-L^3} - E_{KLL} \\ &= (E_K + E_L + U_{KL} - 3E_L - 3U_{LL}) \\ &\quad - (E_K - 2E_L - U_{LL}) = U_{KL} - 2U_{LL}, \quad (18) \end{aligned}$$

where pairwise additivity of the three L final-state holes has been assumed. The latter approximation has been shown to be reasonable for valence holes in atoms and even in molecules and molecular oxyanions.^{1,65,66} In the latter systems, U_{xy} was calculated assuming delocalization of the holes about the molecular system. In the Na-P series, the three core holes are definitely localized on the same atom, however, large interatomic screening effects will definitely reduce the three hole repulsion from the estimate ($3U_{LL}$) dictated by pairwise additivity. Thus interatomic screening will decrease ΔE_{KL-L^3} , which accounts for the smaller experimental shakeoff shifts in Table II. U_{LL} and U_{KL} in Eq. (15) can be estimated from the expressions

$$U_{LL} = E_K - 2E_L - E_{KLL}, \quad (19)$$

$$U_{KL} = E_L^{Z+1} - E_L^Z, \quad (20)$$

utilizing XPS binding energies¹⁰² and the KLL (1D) Auger kinetic energies in Table II. Equation (20) arises in the equivalent cores approximation.⁴⁵

V. SUMMARY AND CONCLUSIONS

We have used a previously published theoretical DOS for Si and a Green's-function approach to distort these DOS appropriate for a screened core hole. We have compared these distorted DOS with XES and AES data to determine the central-cell potentials ϵ_s and ϵ_p , and found that although the s DOS more significantly changes its appearance, more of the charge transfer occurs through the p orbitals. We have used this screened and unscreened DOS and the final-state rule to quantitatively interpret the CCC, CCV, and CVV Auger line shapes of Si. The results of this work lead to the following conclusions.

(1) The KL_1V , $KL_{2,3}V$, and $L_1L_{2,3}V$ line shapes reflect the final-state core-hole screened DOS consistent with the

final-state rule.

(2) The $L_{2,3}VV$ and KVV line shapes are qualitatively different. This difference is discussed in the context of surface effects, intrinsic and extrinsic plasmon losses, and final-state shakeoff.

(3) All features in the $KL_{2,3}L_{2,3}$ line shape of Si are consistent with the same features in the line shapes for Na, Mg, Al, and P.

(4) Core-hole screening (i.e., charge transfer and polarization, initial- and final-state shakeoff from atomic relaxation, and plasmon loss) inherently affects the Auger line shapes of Si, and must be included in a quantitative interpretation of the line shapes.

ACKNOWLEDGMENTS

We acknowledge receiving helpful suggestions from Carter White concerning the theoretical DOS, and from Jim Murday concerning the experimental data in this work. Two of us (F.L.H. and W.N. M.) were partially supported by the U.S. Office of Naval Research.

¹D. E. Ramaker, in *Chemistry and Physics of Solid Surfaces IV*, Vol. 20 of *Springer Series in Chemical Physics*, edited by R. Vanselow and R. Howe (Springer, Berlin, 1982), p. 19.

²D. E. Ramaker, *Phys. Rev. B* **25**, 7341 (1982).

³J. E. Houston, G. Moore, and M. G. Lagally, *Solid State Commun.* **21**, 879 (1977).

⁴P. J. Feibelman, E. J. McGuire, and K. C. Pandey, *Phys. Rev. B* **15**, 2202 (1977); *Phys. Rev. Lett.* **36**, 1154 (1976); P. J. Feibelman and E. J. McGuire, *Phys. Rev. B* **17**, 690 (1978).

⁵R. Weissmann, W. Schnellhammer, R. Koschatzky, and K. Muller, *Appl. Phys.* **14**, 283 (1977).

⁶D. R. Jennison, *Phys. Rev. Lett.* **40**, 807 (1978); *Phys. Rev. B* **18**, 6865 (1978).

⁷R. H. Brockman and G. J. Russell, *Phys. Rev. B* **22**, 6302 (1980).

⁸T. Kunjunny and D. K. Ferry, *Phys. Rev. B* **24**, 4593 (1981); **24**, 4604 (1981).

⁹R. Lasser and J. C. Fuggle, *Phys. Rev. B* **22**, 2637 (1980).

¹⁰N. D. Lang and A. R. Williams, *Phys. Rev. B* **20**, 1369 (1979); **B** **16**, 2408 (1977); A. R. Williams and N. D. Lang, *Phys. Rev. Lett.* **40**, 954 (1978).

¹¹K. Schönhammer and O. Gunnarson, *Solid State Commun.* **23**, 691 (1977).

¹²G. D. Mahan, *Phys. Rev.* **163**, 612 (1967).

¹³J. W. Gadzuk, *J. Electron Spectrosc. Relat. Phenom.* **11**, 355 (1977).

¹⁴D. A. Papaconstantopoulos and E. N. Economou, *Phys. Rev. B* **22**, 2903 (1980).

¹⁵E. N. Economou, *Green's Functions in Quantum Physics*, Vol. 7 of *Springer Series in Solid-State Sciences* (Springer, Berlin, 1979).

¹⁶M. H. Chen, B. Crasemann, and H. Mark, *At. Data Nucl. Data Tables* **24**, 13 (1979); *Phys. Rev. A* **21**, 436 (1980).

¹⁷M. I. Babenkov, B. V. Bobykin, and V. S. Zhdanov, *J. Electron Spectrosc. Relat. Phenom.* **31**, 307 (1983).

¹⁸D. E. Ramaker, J. S. Murday, and N. H. Turner, *J. Electron Spectrosc. Relat. Phenom.* **17**, 45 (1979).

¹⁹H. H. Madden and J. E. Houston, *J. Appl. Phys.* **47**, 3071

(1976).

²⁰R. H. Pratt, *Comm. At. Mol. Phys.* **10**, 121 (1981).

²¹V. S. Sandararn, J. D. Rogers, and R. Landers, *J. Vac. Sci. Technol.* **19**, 117 (1981).

²²J. Cazaux and T. Minh Duc, *J. Electron Spectrosc. Relat. Phenom.* **31**, 13 (1983).

²³U. von Barth and G. Grossman, *Solid State Commun.* **32**, 645 (1979); *Phys. Scr.* **21**, 580 (1980); *Phys. Rev. B* **25**, 5150 (1982); *Phys. Scr.* **28**, 107 (1983).

²⁴G. D. Mahan, *Phys. Rev. B* **21**, 1421 (1980).

²⁵V. I. Grebennikov, Y. A. Babanov, and O. B. Sololov, *Phys. Status Solidi* **80**, 73 (1977).

²⁶L. C. Davis and L. A. Feldkamp, *Phys. Rev. B* **23**, 4269 (1981).

²⁷M. I. Babenkov, B. V. Bobykin, V. S. Zhdanov, and V. K. Petukhov, *Izv. Akad. Nauk* **40**, 2065 (1976).

²⁸L. Asplund, P. Kelfve, B. Blomster, H. Siegbahn, and K. Siegbahn, *Phys. Scr.* **16**, 268 (1977).

²⁹J. J. Mackey, L. E. Smith, B. M. Johnson, C. F. Moore, and D. L. Matthews, *J. Phys. B* **7**, L447 (1974).

³⁰D. L. Walters and C. P. Bhalla, *At. Data* **3**, 301 (1971).

³¹E. J. McGuire, *Phys. Rev. A* **3**, 1801 (1971).

³²M. H. Chen, B. Crasemann, K. N. Huang, M. Aoyagi, and H. Mark, *At. Data. Nucl. Data Tables* **19**, 99 (1977).

³³W. Mehlhorn, *Z. Phys.* **208**, 1 (1968).

³⁴E. J. McGuire, *Phys. Rev. A* **11**, 1880 (1975).

³⁵C. P. Bhalla, *Phys. Lett.* **44A**, 103 (1973).

³⁶D. Chattarji and B. Talukdar, *Phys. Rev. A* **7**, 42 (1973).

³⁷M. H. Chen, B. Crasemann, and H. Mark, *Phys. Rev. A* **8**, 7 (1973).

³⁸M. H. Chen, B. Crasemann, and H. Mark, *Phys. Rev. A* **21**, 442 (1980).

³⁹E. J. McGuire, *Phys. Rev.* **185**, 1 (1969); Sandia Laboratory Research Report No. SC-RR-710075, March, 1971 (unpublished); *Phys. Rev. A* **2**, 273 (1970); **3**, 587 (1971).

⁴⁰D. L. Walters and C. P. Bhalla, *Phys. Rev. A* **4**, 2164 (1971).

⁴¹G. Wiech and E. Zopf, in *Band-Structure Spectroscopy of Metals and Alloys*, edited by D. J. Fabian and L. M. Watson

- (Academic, London, 1973), p. 173.
- ⁴²L. Ley, F. R. McFeely, S. P. Kowalczyk, J. G. Jenkin, and D. A. Shirley, *Phys. Rev. B* **11**, 600 (1975); R. Fellenberg, P. Streubel, and A. Meisel, *Phys. Status Solidi B* **112**, 55 (1982).
- ⁴³W. F. Hanson and E. T. Arakawa, *Z. Phys.* **251**, 271 (1972).
- ⁴⁴C. Cini and A. D'Andrea, *J. Phys. C* **41**, 4469 (1983).
- ⁴⁵W. L. Jolly and D. N. Hendrickson, *J. Am. Chem. Soc.* **92**, 1863 (1970).
- ⁴⁶J. D. Dow, D. R. Franceschetti, P. C. Gibbons, and S. E. Schnatterly, *J. Phys. F* **5**, L211 (1975).
- ⁴⁷R. L. Aggarawal, P. Fisher, V. Mourzine, and A. K. Ramdas, *Phys. Rev.* **138A**, 882 (1965).
- ⁴⁸F. C. Brown and O. P. Rustgi, *Phys. Rev. Lett.* **28**, 497 (1972); M. L. Knotek, G. M. Loubriel, R. H. Stulen, C. E. Parks, B. E. Koel, and Z. Hussain, *Phys. Rev. B* **26**, 2292 (1982).
- ⁴⁹G. Margaritondo and J. E. Rowe, *Phys. Lett.* **59A**, 464 (1977); R. S. Bauer, R. Z. Bachrach, D. E. Aspnes, and J. C. McMenamin, *Nuovo Cimento B* **39**, 464 (1977).
- ⁵⁰K. L. Kobayashi, H. Daimon, and Y. Murata, *Phys. Rev. Lett.* **50**, 1701 (1983); **52**, 1569 (1984); R. A. Riedel, M. Turowski, G. Margaritondo, and P. Perfetti, *Phys. Rev. Lett.* **52**, 1568 (1984).
- ⁵¹H. P. Hjalmarson, P. Vogl, D. J. Wolford, and J. D. Dow, *Phys. Rev. Lett.* **44**, 810 (1980); H. P. Hjalmarson, H. Buttner, and J. D. Dow, *Phys. Rev. B* **24**, 6010 (1981).
- ⁵²L. Resca, L. Resta, and B. Shore, *Phys. Rev. B* **25**, 4031 (1982); L. Resca and R. Resta, *ibid.* **25**, 4038 (1982).
- ⁵³A. Zunger, *Phys. Rev. Lett.* **50**, 1215 (1983); V. A. Singh, A. Zunger, and V. Lindefelt, *Phys. Rev. B* **27**, 1420 (1983).
- ⁵⁴G. Strinati, *Phys. Rev. Lett.* **49**, 1519 (1982).
- ⁵⁵F. Bechstedt, R. Enderlein, R. Fellenberg, P. Streubel, and A. Meisel, *J. Electron Spectrosc. Relat. Phenom.* **31**, 131 (1983).
- ⁵⁶D. A. Shirley, *Phys. Rev. A* **7**, 1520 (1973); *Chem. Phys. Lett.* **17**, 312 (1972).
- ⁵⁷J. A. Taylor, *Appl. Surf. Sci.* **7**, 168 (1981).
- ⁵⁸D. E. Ramaker, F. L. Hutson, R. R. Rye, J. E. Houston, and J. W. Rogers, Jr., *J. Vac. Sci. Technol. A* **2**, 1146 (1984); and unpublished.
- ⁵⁹P. Pehrsson and D. E. Ramaker (unpublished).
- ⁶⁰C. J. Powell, *Phys. Rev. Lett.* **30**, 1179 (1973).
- ⁶¹J. W. Gadzuk, *Phys. Rev. B* **9**, 1978 (1974).
- ⁶²J. E. Houston, *J. Vac. Sci. Technol.* **12**, 255 (1973).
- ⁶³J. Fitchek and S. M. Bose, *Phys. Lett.* **54A**, 460 (1975).
- ⁶⁴J. R. Chelikowsky and M. L. Cohen, *Phys. Rev. B* **10**, 5095 (1974).
- ⁶⁵F. L. Hutson, D. E. Ramaker, B. I. Dunlap, J. D. Ganjei, and J. S. Murday, *J. Chem. Phys.* **76**, 2181 (1981).
- ⁶⁶B. I. Dunlap, F. L. Hutson, and D. E. Ramaker, *J. Vac. Sci. Technol.* **18**, 556 (1981).
- ⁶⁷S. D. Bader, L. Richter, and M. B. Brodsky, *Solid State Commun.* **37**, 729 (1981).
- ⁶⁸G. W. Rubloff, P. S. Ho, J. F. Freeouf, and J. E. Lewis, *Phys. Rev. B* **23**, 4183 (1981).
- ⁶⁹D. E. Ramaker, W. N. Mei, and N. H. Turner, *J. Vac. Sci. Technol.* **20**, 563 (1982).
- ⁷⁰M. Davies, D. R. Jennison, and P. Weightman, *J. Phys. C* **17**, L107 (1984); *Phys. Rev. B* **29**, 5313 (1984); M. Davies, P. H. Hannah, P. Weightman, and P. T. Andrews, *J. Phys. F* **14**, 355 (1984); D. R. Jennison, P. Weightman, P. Hannah, and M. Davies, *J. Phys. C* **17**, 3701 (1984).
- ⁷¹M. Cini and A. D'Andrea, *Phys. Rev. B* **29**, 6540 (1984); M. Cini, *ibid.* **17**, 2486 (1978).
- ⁷²A. M. Baro and J. A. Tagle, *J. Phys. F* **8**, 563 (1978).
- ⁷³R. P. Gupta and A. J. Freeman, *Phys. Rev. Lett.* **36**, 1194 (1976); P. H. Citrin, G. K. Wertheim, and M. Schlüter, *Phys. Rev. B* **20**, 3067 (1979).
- ⁷⁴M. Taniguchi, S. Suga, M. Seki, H. Sakamoto, H. Kanzaki, Y. Akahama, S. Endo, S. Terada, and S. Narita, *Solid State Commun.* **49**, 867 (1984).
- ⁷⁵M. O. Krause, T. A. Carlson, and R. D. Dismukes, *Phys. Rev.* **170**, 37 (1968); T. A. Carlson, *Radiat. Res.* **64**, 53 (1975).
- ⁷⁶D. Haneman, *Phys. Rev.* **121**, 1093 (1961); D. J. Miller and D. Haneman, *J. Vac. Sci. Technol.* **16**, 1270 (1979).
- ⁷⁷P. Morgen and J. Onsgaard, *Surf. Sci.* **99**, 87 (1980); P. Morgen and F. Ryborg, *J. Vac. Sci. Technol.* **17**, 578 (1980).
- ⁷⁸M. C. Muñoz, V. Martinez, J. A. Tagle, and J. L. Sacedon, *Phys. Rev. Lett.* **44**, 814 (1980).
- ⁷⁹G. De Meyer, R. Hoogewijs, W. Lambrecht, and J. Vennik, *Solid State Commun.* **33**, 267 (1980).
- ⁸⁰M. L. Knotek and J. E. Houston, *J. Vac. Sci. Technol.* **20**, 544 (1982).
- ⁸¹M. P. Seah, National Physical Laboratory Report No. DMA(A) 40, February, 1982 (unpublished).
- ⁸²N. H. Turner and D. E. Ramaker, *J. Vac. Sci. Technol.* **1**, 1229 (1983).
- ⁸³B. Breuckmann, *J. Phys. B* **12**, L609 (1979).
- ⁸⁴E. Brueckmann, B. Breuckmann, W. Mehlhorn, and W. Schmitz, *J. Phys. B* **10**, 3135 (1977).
- ⁸⁵D. Petrini, *Astron. Astrophys.* **111**, 279 (1982).
- ⁸⁶B. Breuckmann and V. Schmidt, *Z. Phys.* **268**, 235 (1974); B. Breuckmann, V. Schmidt, and W. Schmitz, *J. Phys. B* **9**, 3037 (1976).
- ⁸⁷N. Kosugi and H. Kuroda, *Chem. Phys. Lett.* **87**, 365 (1982).
- ⁸⁸T. A. Carlson, C. W. Nestor, Jr., T. C. Tucker, and F. B. Malik, *Phys. Rev.* **169**, 27 (1968).
- ⁸⁹J. Stohr, R. Jaeger, and J. J. Rehr, *Phys. Rev. Lett.* **51**, 821 (1983); T. D. Thomas, *Phys. Rev. Lett.* **52**, 417 (1984).
- ⁹⁰A. Barrie and F. J. Street, *J. Electron Spectrosc. Relat. Phenom.* **7**, 1 (1975).
- ⁹¹P. M. Th. M. van Attekum and J. M. Trooster, *Phys. Rev. B* **20**, 2335 (1979).
- ⁹²A. Fahlman, R. Nordberg, C. Nordling, and K. Siegbahn, *Z. Phys.* **192**, 476 (1966).
- ⁹³J. C. Fuggle, L. M. Watson, D. J. Fabian, and S. Affrossman, *J. Phys. F* **5**, 375 (1975).
- ⁹⁴P. M. Th. M. van Attekum and J. M. Trooster, *Phys. Rev. B* **18**, 3872 (1978).
- ⁹⁵M. Scharli and J. Brunner, *Z. Phys. B* **42**, 285 (1981).
- ⁹⁶H. J. Freund, E. W. Plummer, W. R. Salaneck, and R. W. Bigelow, *J. Chem. Phys.* **75**, 4275 (1981).
- ⁹⁷D. A. Shirley, *Phys. Rev. A* **9**, 1549 (1974).
- ⁹⁸R. Hoogewijs, L. Fiermans, and J. Vennik, *J. Electron Spectrosc. Relat. Phenom.* **11**, 171 (1977).
- ⁹⁹G. Dufour, J. M. Mariot, P. E. N. Jatko, and R. C. Karnatak, *Phys. Scr.* **13**, 370 (1976).
- ¹⁰⁰M. H. Chen and B. Crasemann, *Phys. Rev. A* **8**, 7 (1973).
- ¹⁰¹C. D. Wagner, D. E. Passoja, H. F. Hillery, T. J. Kinisky, H. A. Six, W. T. Jansen, and J. A. Taylor, *J. Vac. Sci. Technol.* **21**, 933 (1982).
- ¹⁰²J. C. Fuggle and N. Martensson, *J. Electron Spectrosc. Relat. Phenom.* **21**, 275 (1980).